



Article

Solvent- and Light-Sensitive AIEE-Active Azo Dye: From Spherical to 1D and 2D Assemblies

Mina Han ^{1,*}, Ikue Abe ², Jihun Oh ³, Jaehoon Jung ^{3,*} , Young Ji Son ⁴, Jaegeun Noh ⁴, Mitsuo Hara ⁵ and Takahiro Seki ⁵

¹ Department of Chemistry Education, Kongju National University, Gongju 32588, Korea

² Department of Chemistry and Biotechnology, Graduate School of Engineering, Tottori University, Tottori 680-8552, Japan; hibari1116@gmail.com

³ Department of Chemistry, University of Ulsan, Ulsan 44776, Korea; gminor231@gmail.com

⁴ Department of Chemistry, Institute of Nano Science and Technology, Hanyang University, 222 Wangsimni-ro, Seongdong-gu, Seoul 04763, Korea; syj2010@hanyang.ac.kr (Y.J.S.); jgnoh@hanyang.ac.kr (J.N.)

⁵ Department of Molecular and Macromolecular Chemistry, Graduate School of Engineering, Nagoya University, Furo-cho, Chikusa-ku, Nagoya 464-8603, Japan; mhara@chembio.nagoya-u.ac.jp (M.H.); tseki@chembio.nagoya-u.ac.jp (T.S.)

* Correspondence: hanmin@kongju.ac.kr (M.H.); jjung2015@ulsan.ac.kr (J.J.)

Abstract: Fluorescent molecular assembly systems provide an exciting platform for creating stimuli-responsive nano- and microstructured materials with optical, electronic, and sensing functions. To understand the relationship between (i) the plausible molecular structures preferentially adopted depending on the solvent polarity (such as *N,N*-dimethylformamide [DMF], tetrahydrofuran [THF], and toluene), (ii) the resulting spectroscopic features, and (iii) self-assembled nano-, micro-, and macrostructures, we chose a sterically crowded triangular azo dye (3Bu) composed of a polar molecular core and three peripheral biphenyl wings. The chromophore changed the solution color from yellow to pink-red depending on the solvent polarity. In a yellow DMF solution, a considerable amount of the twisted azo form could be kept stable with the help of favorable intermolecular interactions with the solvent molecules. By varying the concentration of the DMF solution, the morphology of self-assembled structures was transformed from nanoparticles to micrometer-sized one-dimensional (1D) structures such as sticks and fibers. In a pink-red toluene solution, the periphery of the central ring became more planar. The resulting significant amount of the keto-hydrazone tautomer grew into micro- and millimeter-sized 1D structures. Interestingly, when THF-H₂O (1:1) mixtures were stored at a low temperature, elongated fibers were stacked sideways and eventually developed into anisotropic two-dimensional (2D) sheets. Notably, subsequent exposure of visible-light-irradiated sphere samples to solvent vapor resulted in reversible fluorescence off↔on switching accompanied by morphological restoration. These findings suggest that rational selection of organic dyes, solvents, and light is important for developing reusable fluorescent materials.

Keywords: triangular azo dye; light and solvent response; molecular assembly; morphological transformation



Citation: Han, M.; Abe, I.; Oh, J.; Jung, J.; Son, Y.J.; Noh, J.; Hara, M.; Seki, T. Solvent- and Light-Sensitive AIEE-Active Azo Dye: From Spherical to 1D and 2D Assemblies. *Int. J. Mol. Sci.* **2022**, *23*, 965. <https://doi.org/10.3390/ijms23020965>

Academic Editor: Mihai V. Putz

Received: 21 December 2021

Accepted: 14 January 2022

Published: 16 January 2022

Publisher's Note: MDPI stays neutral with regard to jurisdictional claims in published maps and institutional affiliations.



Copyright: © 2022 by the authors. Licensee MDPI, Basel, Switzerland. This article is an open access article distributed under the terms and conditions of the Creative Commons Attribution (CC BY) license (<https://creativecommons.org/licenses/by/4.0/>).

1. Introduction

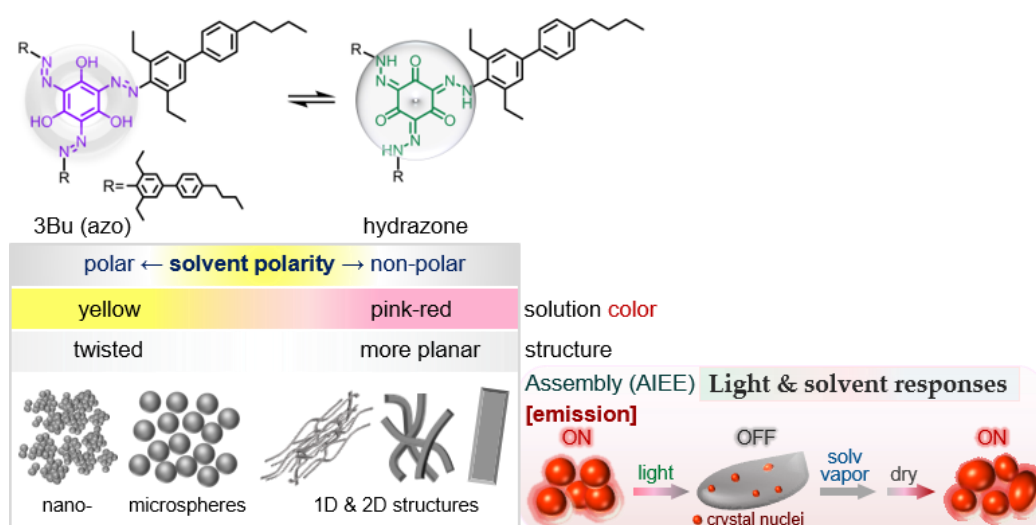
Fluorescent molecular assembly systems provide an exciting platform for constructing reversibly stimuli-responsive assembled nano- and microstructures whose optical, electronic, and sensing functions can be regulated by contact and non-contact stimuli such as light, chemicals, temperature, and pressure [1–25]. Many studies have reported the self-assembly of π -conjugated organic chromophores into versatile fluorescent nano- and microstructured materials with such desired functions [1–6,12,14,21]. A sufficient understanding of (i) the design of small component molecules, (ii) specific and non-specific interactions of the molecules with surrounding solvents, and (iii) three-dimensional molecular arrangements is critical to elicit responses to stimuli from the self-assembled systems.

For instance, the introduction of bulky substituents restricts the free rotation around a single or double bond, thus changing the twisting degree of the planar geometry. Such sterically crowded chromophores often undergo specific interactions with solvents with different polarities, and the resulting conformational and tautomeric structures may affect not only spectroscopic (absorption and emission) and sensing features but also molecular assemblies [26–37].

Azobenzene is a well-known photo-responsive compound, but is generally known to not emit with appreciable quantum yield ($\sim 10^{-7}$ – 10^{-5}) [38–43]. This is because the energy in the excited state is highly consumed through nonradiative conformational changes, thus reducing the fluorescence intensity significantly. However, Kawashima et al. developed intensely fluorescent boron-substituted azobenzenes [44–46]. The intramolecularly strong B–N interaction disrupts the molecular structural changes around the azo group, which is mainly responsible for the high fluorescence efficiency. Yoon et al. examined the aggregation-induced emission enhancement (AIEE [47–52]) property of *o*-phenylazonaphthol (*o*-PAN)-based chromophores [53]. The planarization associated with strong intramolecular hydrogen bonding and the restriction of intramolecular rotation in the hydrazone tautomer form are likely responsible for the enhanced fluorescence. Recently, Yamauchi and coworkers introduced a pyrene-functionalized azobenzene derivative with crystallization-induced emission (CIE) or AIEE characteristics associated with the suppression of photoisomerization [54]. Caruso and coworkers synthesized symmetric bis-azobenzene red dyes with relevant fluorescence quantum yield in the solid state [55]. Lee et al. synthesized torsionally responsive C_3 -symmetric azo dyes and characterized in detail their reversible conformational switching through twisting of C–N bonds, based on their experimental and computational studies [56].

Nevertheless, there are limited examples of light- and solvent-responsive assembled nano- and microstructures that express both light-driven phase transition and reversible fluorescence on \leftrightarrow off switching functions [57–62]. We recently reported that a triangular azo dye designed with consideration of rigidity and flexibility displayed remarkable AIEE and light-induced conformational change from the symmetric to asymmetric structure [60]. However, neither morphological recovery to the original spherical shape nor reversible fluorescence switching was achieved by external stimuli such as light, heat, or pressure.

Here, we describe the relationship between (i) the plausible conformational and tautomeric structure in which a sterically crowded triangular chromophore (3Bu, Scheme 1) is preferentially adopted depending on the solvent polarity and concentration, (ii) the resulting spectroscopic features, and (iii) the morphology of self-assembled nano-, micro-, and macrostructures formed in various mixed solutions. 3Bu changed the solution color from yellow to pink-red depending on the solvent polarity. A very dilute solution prepared with a more polar solvent such as DMF was yellow, and appeared to contain a significant quantity of a twisted azo form. The highly twisted conformation tended to assemble into less ordered spherical nanoparticles or micrometer-sized spheres showing AIEE characteristics. In contrast, when dissolved in a non-polar solvent such as toluene, the central ring core had a more planar conformation. The resulting keto-hydrazone tautomer grew into micro- and millimeter-sized one-dimensional (1D) structures. Moreover, when a visible-light-irradiated sample was exposed to organic solvent vapors, reverse fluorescence off-to-on switching was realized with recovery of the original morphology.



Scheme 1. Upper: Chemical structure. Lower left: The plausible molecular structure preferentially taken under different solvent conditions, the resulting solution color, and the morphology of self-assembled structures. Lower right: Light and solvent responses: Subsequent exposure of a light-irradiated sphere sample to solvent vapor resulted in reversible fluorescence off↔on switching accompanied by recovery of the round shape.

2. Results and Discussion

2.1. Solvent Effect

Sterically crowded 3Bu was thermally stable up to ~ 210 °C (Figure S1) and dissolved well in common organic solvents such as chloroform, toluene, tetrahydrofuran (THF), and *N,N*-dimethylformamide (DMF) to make transparent solutions, and the color of the solution observed by the naked eye varied from yellow to pink-red depending on the solvent polarities (Figure 1). A dilute 3Bu DMF solution was yellow, and its UV-vis absorption spectrum contained both a weak shoulder in the region of 330–400 nm and a strong absorption band centered at around 442 nm. This unusual absorption band was presumably due not only to the energetic similarity between the low-lying (π, π^*) and (n, π^*) states associated with the charge transfer character in the long conjugated system but also to the twisted azobenzene-based $n-\pi^*$ transition [63–66]. The reason why the molecular central ring connected with three hydroxyl (–OH) groups can adopt a twisted conformation is that three bulky biphenyl wings are directly linked to the central ring via azo (–N=N–) groups. This twisted conformer could possibly be maintained with the help of intermolecular interactions with surrounding polar solvent molecules.

Unlike the absorption spectrum of the yellow DMF solutions, two characteristic absorption bands with maximum values at around 381 and 504 nm appeared in the absorption spectrum for a less polar THF solution. Moreover, upon dissolving in non-polar toluene, the dilute solution showed a bright pink-red color, and two intense absorption bands were red-shifted to 384 and 515 nm, respectively (Figure 1a and Table 1). That is, 3Bu is a negatively solvatochromic compound [26–31].

These absorption spectral changes depending on the solvent polarity can be interpreted as follows [67–71]. Non-polar toluene molecules would interact even better with three biphenyl wings than the polar molecular core. It is likely advantageous for the molecular core to adopt a more planar conformation, thereby facilitating intramolecular hydrogen bond formation and proton transfer from the hydroxyl group to the nitrogen atom. The resulting keto-hydrazone form is presumably responsible for the characteristic absorption bands appearing in the long wavelength region above 500 nm. In addition, non-polar toluene solutions in a concentration range from ~ 0.3 μM to ~ 30 μM showed almost the same maximum absorption values (Figure 1b).

In contrast to the toluene solution, which was negligibly affected by concentration, the absorption spectra of polar DMF solutions were sensitive to 3Bu concentration. For instance, unlike the quite dilute solution ($\leq 10 \mu\text{M}$), a more concentrated solution ($\geq 20 \mu\text{M}$) had a maximum absorption band at $\sim 470\text{--}480 \text{ nm}$ together with a considerably broad shoulder in the $360\text{--}450 \text{ nm}$ region (Figure 1a,d and Table 1). To further verify gradual molecular structural changes depending on the solvent polarity, absorption spectroscopic measurements were performed by varying the ratio of DMF and toluene at the same concentration of $20 \mu\text{M}$ (Figure S2). As expected, with increasing toluene content, the broad shoulder in the $360\text{--}440 \text{ nm}$ region decreased, and instead, two absorption bands maximized at approximately 380 and 510 nm clearly emerged. Notably, as the toluene fraction (f_{tol}) was increased to 80% , the absorption spectrum was almost the same as that of the sample with $f_{\text{tol}} = 100\%$. These results suggest that a change in the DMF-toluene mixing ratio created a gradual transition from a twisted to a more planar structure, which in turn promoted the conversion to the keto-hydrazone form.

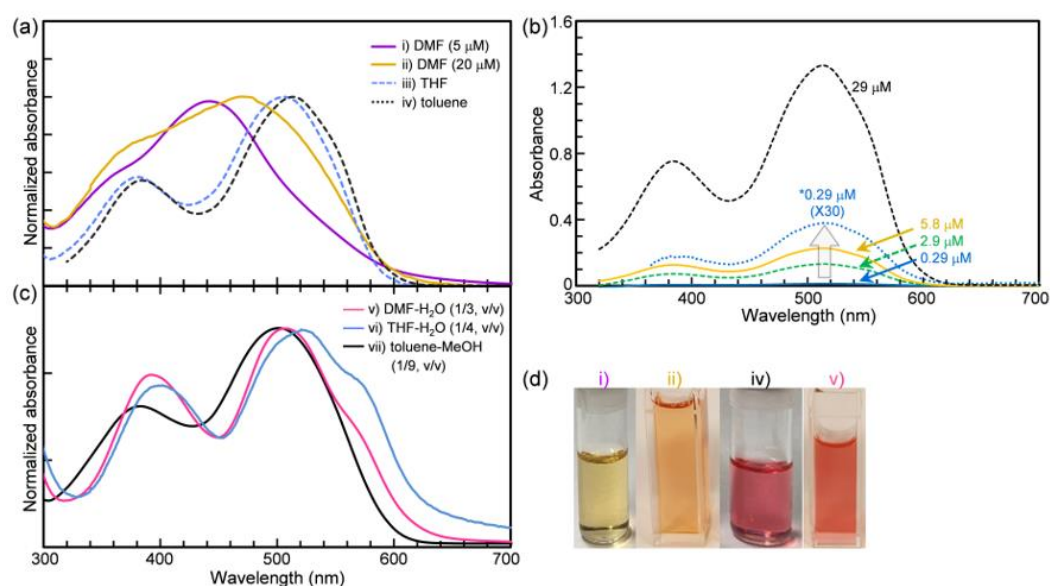


Figure 1. Normalized UV-vis absorption spectra for 3Bu (a) in solvents with different polarities and (c) in mixed solutions. (b) Absorption spectra of 3Bu toluene solutions measured in concentration range from 0.29 to $29 \mu\text{M}$. (d) Photograph of 3Bu in (i) DMF ($5 \mu\text{M}$), (ii) DMF ($20 \mu\text{M}$), (iv) toluene, and (v) DMF- H_2O mixture. All solutions except for DMF in (a) and toluene in (b) had a concentration of $10 \mu\text{M}$. See Table 1, also.

Table 1. Solvent properties, spectroscopic data, and self-assembled structures of 3Bu obtained from various solvent environments.

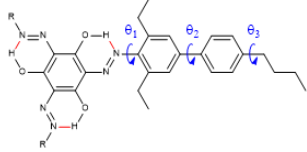
Solvent	DMF	DMF- H_2O	THF	THF- H_2O	Toluene	Toluene-MeOH
polarity	13.7	-	5.7	-	1.4	-
dielectric constant	38.2	-	7.5	-	2.4	-
$\lambda_{\text{max}}^{\text{abs}}$	442→470–480	392, 505	381, 504	400, 517	384, 515	383, 502
$\lambda_{\text{max}}^{\text{em}}$	608	632	610	629	616	617
aggregate morphology	-	nanoparticle→1D structures	-	sphere (1D→2D structures)	-	1D structures
AIEE property	-	○	-	○	-	○

2.2. Theoretical Calculations

In order to understand the solvatochromism of the 3Bu molecule, density functional theory (DFT) calculations were carried out using a B3LYP functional [72] and 6-31G(d,p)

basis set implemented in the Gaussian 09 software package [73]. The influence of a different solvent medium on the geometric and electronic structures was examined using an SMD model within self-consistent reaction field (SCRF) approximation [74]. The most stable geometry had approximately C_3 symmetry regardless of solvent polarity, although the symmetry constraint was not considered during geometry optimizations (Figure 2a). The azo groups were located in the same plane as the central benzene ring due to the intramolecular hydrogen bonding and π -conjugation. The intramolecular hydrogen bonding distances were ~ 1.56 Å for all solvent mediums. However, the planarity of the 3Bu molecule showed a considerable change depending on the polarity of the solvent medium despite the approximated consideration of the solvent medium (Figure 2b). As the polarity decreased (DMF > THF > toluene), the displacement of ethyl groups from the molecular plane increased, and they were attached to the first benzene ring of the side group. We examined the variation of molecular planarity with the torsional angle (θ_1) between the azo group and the first benzene ring of a side chain and identified the orientation of the side group with three torsional angles (inset figure in Table 2), while the torsional angles θ_2 and θ_3 were almost identical for all solvent mediums, and the torsional angle θ_1 gradually decreased (i.e., the planarity increased) as the solvent polarity decreased (Table 2). The frontier molecular orbitals, mainly characterized as π -orbitals, were dominantly distributed from the central benzene ring to the first benzene ring of the side group (Figure 2c). Therefore, the energy gap between the highest occupied and the lowest unoccupied molecular orbitals (HOMO-LUMO gap) was highly influenced by the variation of the torsional angle θ_1 , and thus a larger HOMO-LUMO gap was obtained for a more highly polar solvent (Table 2), which agrees quite well with the experimental observation (see Figure 1). Time-dependent DFT (TD-DFT) calculations were further performed to reveal the solvatochromism of the 3Bu molecule. The computationally obtained absorption wavelength (λ_{\max} for $S_1 \leftarrow S_0$) was also roughly comparable to the HOMO-LUMO gap and experimental results (Table 2).

Table 2. Computationally obtained average dihedral angles, HOMO-LUMO gaps, and absorption wavelengths depending on solvent medium. Inset: Two-dimensional structural skeleton of 3Bu, where intramolecular hydrogen bonds are red-colored and three torsional angles are blue-colored.

Solvent	DMF	THF	Toluene
Average dihedral angle ($^\circ$)			
 θ_1	27.1	18.5	13.3
θ_2	−34.2	−34.8	−35.4
θ_3	89.7	89.7	88.9
HOMO-LUMO gap (eV)	3.12	2.35	2.25
Abs. wavelength (λ_{\max} , nm)	473.9	491.8	497.2

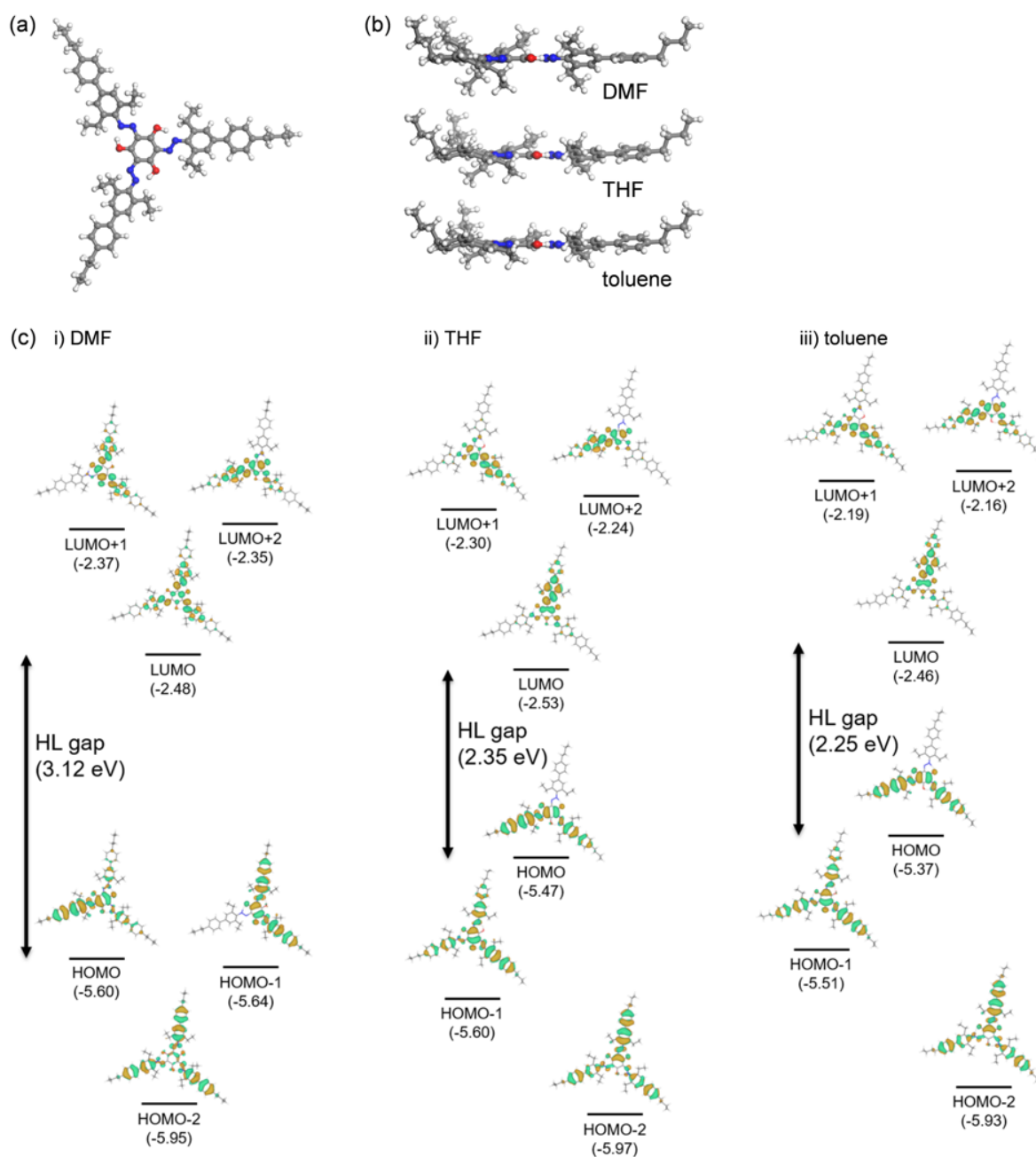


Figure 2. (a) Top view of 3Bu molecule optimized in DMF. (b) Side views of optimized 3Bu molecules in different solvent media. (c) Computationally estimated energy diagram for the frontier molecular orbitals of 3Bu molecule in different solvent media, the influence of which was accounted for using SCRF approximation.

2.3. Self-Assembly into Spherical and 1D Structures

To investigate how such delicate changes in conformational or tautomeric structures affect their molecular assemblies and the resulting spectroscopic features, we next produced self-assembled nano- and microstructures using a reprecipitation method. Figure 3 shows the absorption and fluorescence spectral changes of 3Bu DMF-H₂O mixtures prepared by varying the water fraction while keeping the concentrations at 10 μ M. As soon as a few drops of ultrapure water, which is a poor solvent, were added into a 3Bu DMF solution under gentle shaking, the color of the mixed solution dramatically changed from yellow to bright red, which could be clearly observed with the naked eye (inset photo in

Figure 1d). The characteristic absorption band at ~ 442 nm disappeared completely, and two intense absorption bands at ~ 392 and 505 nm emerged (Figure 3a). At the same time, the maximum fluorescence wavelength was red-shifted from 608 nm to 630 nm, and the intensity increased considerably (Figure 3b,c). As the water fraction was increased to 75% , the fluorescence intensity reached the maximum, which was about 7.5 times higher than that of the dilute DMF solution. These results support that 3Bu is AIEE-active [47–52]. Our careful scanning electron microscopy (SEM) observations revealed the formation of nanometer-sized spherical particles with diameters of ~ 10 – 100 nm (Figure 4a). Such small aggregates were often found as agglomerates rather than being dispersed on the hydrophilic glass substrate. In addition, a turbid suspension produced by adding H_2O to a less polar THF solution displayed absorption maxima at 400 and 517 nm (Figure 1c). Micrometer-sized spheres with sizes of ~ 0.1 – 1.0 μm were found in the concentration range of 1.0 – 25 μM (Figure 4b).

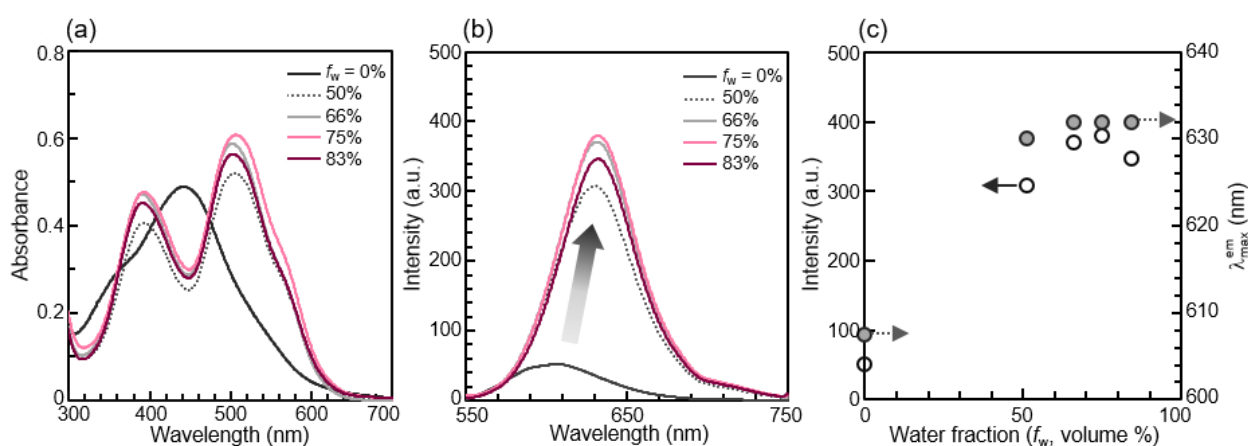


Figure 3. (a) Absorption and (b) fluorescence ($\lambda_{ex} = 510$ nm) spectra of 3Bu in DMF- H_2O mixed solutions (10 μM) prepared by varying the water fraction (f_w). (c) Changes in the fluorescence intensity at the maximum fluorescence wavelength as a function of f_w .

Unlike the dilute DMF- H_2O mixtures, mixed solutions with concentrations of 50 μM or higher did not become turbid, but rather, insoluble floats were generated and gradually sank to the bottom of a quartz cuvette with a 10 mm path length. The SEM images presented in Figure 4c verify the coexistence of long sticks and intertwined fibers with length of tens of micrometers instead of spheres. In other words, the morphological transformation from nanoparticles to micrometer-sized 1D structures was realized simply by varying the concentration.

In toluene-MeOH mixed solutions, cotton-like precipitates were very slowly produced over 1 to 3 weeks without becoming turbid and slowly separated from the transparent solution. Figure 4d and Figure S3 show that such fluffy precipitates were composed of both long sticks hundreds of micrometers in length and elongated fibers that were several millimeters long. The respective 1D structures were red fluorescent upon excitation with green light (Figure S3b). As evidenced by our SEM observations, the fibrous structures appeared to be flexible and were often broken into two or more pieces, suggesting that they were crystalline.

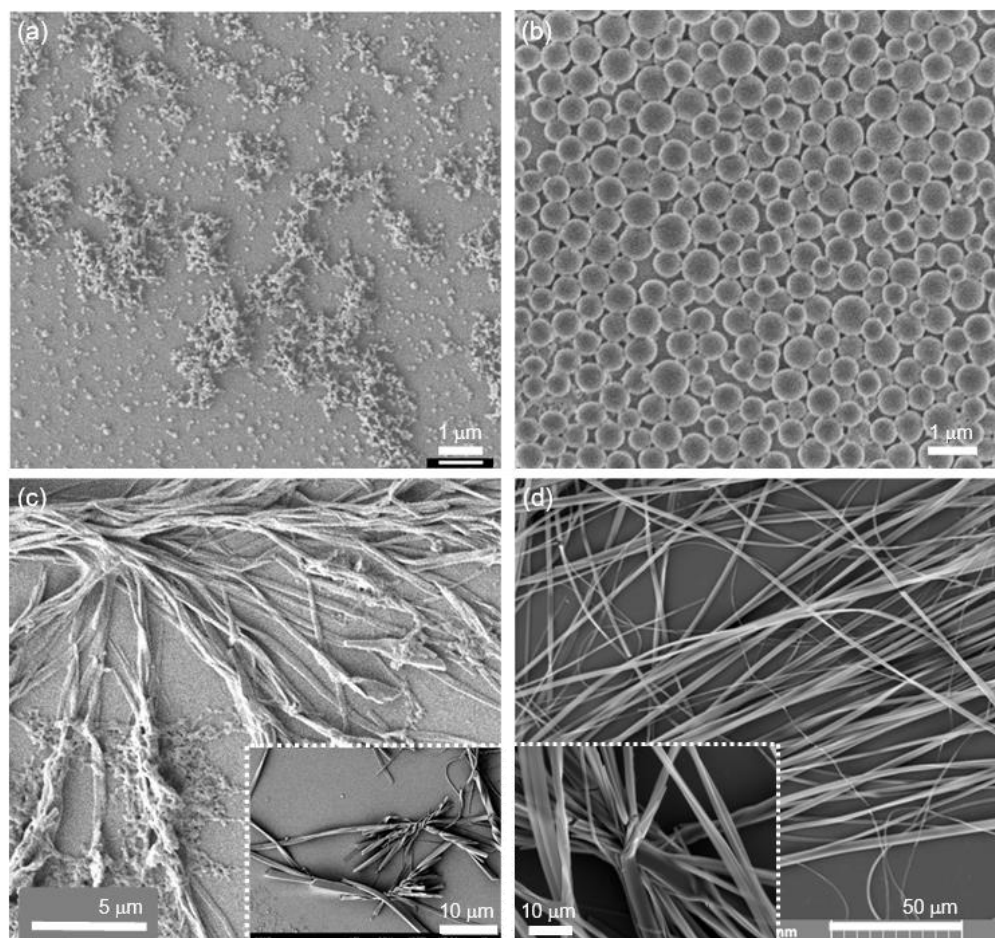


Figure 4. SEM images of self-assembled structures obtained from (a) DMF-H₂O (1/3, *v/v*, 10 μM), (b) THF-H₂O (1/4, *v/v*, 20 μM), (c) DMF-H₂O (1/1, *v/v*, 100 μM), and (d) toluene-MeOH (1/4, *v/v*, 100 μM) mixtures.

2.4. Coexistence of Spherical, 1D and 2D Structures

Surprisingly, in the case of a 25 μM THF-H₂O (1/1, *v/v*) mixed solution, when the turbid mixture was stored at 10–15 °C, unlike other ratios in which turbid mixed solutions remained stable, visible floats were produced. They gradually sank to the bottom of the quartz cell, and as a result, the solution became transparent. The OM and FOM images of the precipitates reveal that light purple rectangular aggregates with red fluorescence coexisted with long, flat belts of dark purple color (Figure 5a,b). Uneven ends and corners were frequently found in the OM, atomic force microscopy (AFM), and SEM images (Figures 5 and 6), and the samples may have been torn during growth or during their preparation. Their thickness and width were approximately 60–100 nm and 1–20 μm, respectively. AFM topographic images obtained for sheets exhibited uneven surfaces regardless of their size (Figure 5c,d). Very tiny spherical nanoparticles of approximately 10–20 nm in height were frequently observed on such sheet surfaces (Figure 5d). Notably, from polarized optical microscopy (POM) images measured under crossed Nicol conditions, when the long axis of the rectangular sheet was placed at approximately 45° (Figure 6c,i) and 0° (Figure 6f) with respect to both the polarizer and analyzer, it was observed to be maximally bright and maximally dark, respectively [75–78]. These data support that the triangular molecules were well aligned in the long axis direction (in-plane alignment) to form anisotropic sheets.

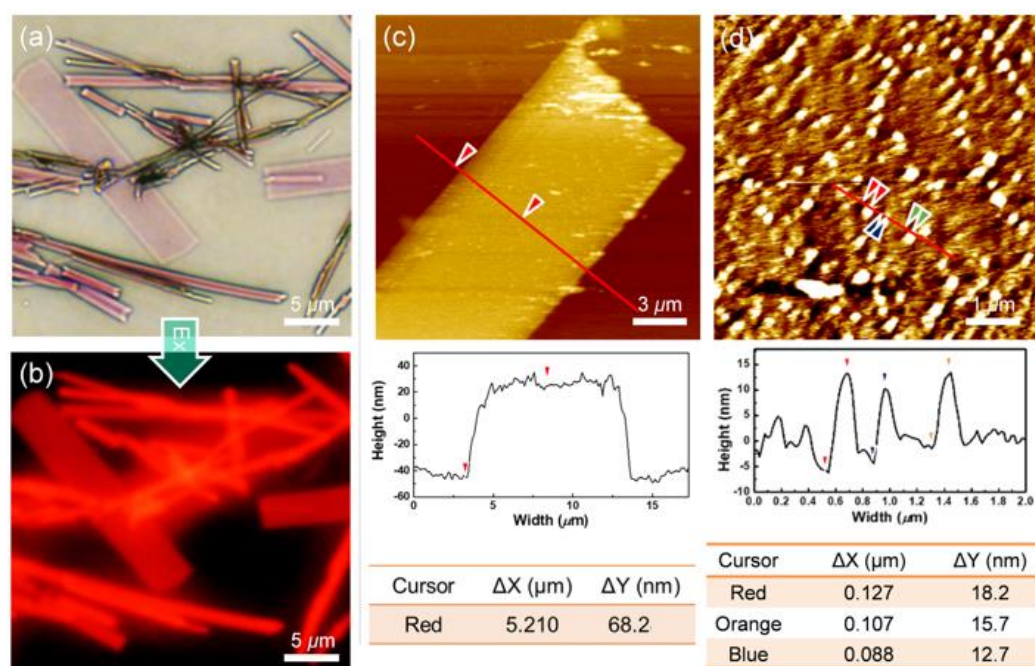


Figure 5. (a) OM and (b) FOM images of 3Bu belts and sheets obtained from 25 μM THF-H₂O (1/1, *v/v*) at 10–15 °C. (c) AFM image showing 3Bu microsHEET on a glass substrate and height profile. (d) Magnified AFM image showing spherical nanoparticles on 3Bu microsHEET and height profile.

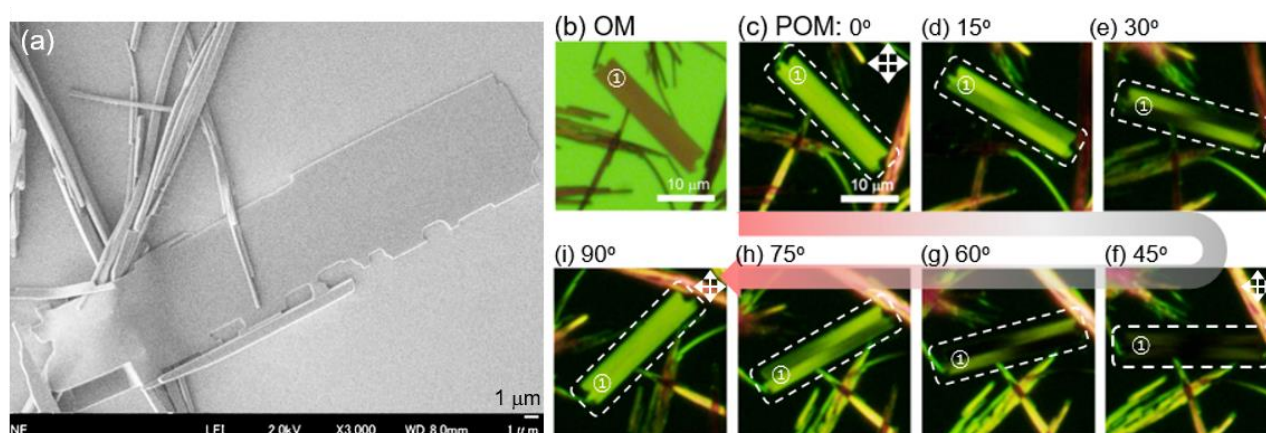


Figure 6. (a) SEM image of belts and sheets prepared from 25 μM THF-H₂O (1/1, *v/v*) at 10–15 °C. (b) OM and (c–i) POM images of birefringent microsheets placed between the crossed polarizers. The sample direction was rotated by 15 degrees with respect to the crossed polarizers.

Additional OM and SEM observations were carried out to obtain insight into the growth process of fluorescent anisotropic sheets. Upon addition of water to the THF solution, purple agglomerates of approximately 20 μm or less, interconnected by elongated fibers, were frequently found along with spherical particles with a diameter of approximately 500 nm or less (Figure 7a). As time passed, these fibers began to pile up sideways, reaching a width of several hundred nanometers to several micrometers (Figures 7b and S4a). The OM and SEM images in Figures 7c and S4b show that they grew into branches and belts. After about 2–4 h, they developed into micrometer-sized sheets, and gradually sank to the bottom along with long belts (Figure 7d–e). The growth process of the 2D structures through the lateral stacking of 1D fibers is likely responsible for the strong birefringence of micrometer-sized sheets. Although it is still unknown why 1D fibers

prefer such lateral stacking, low temperature and the mixing ratio of the solvents appear to be important factors in developing spherical and 1D structures into fluorescent 2D sheets.

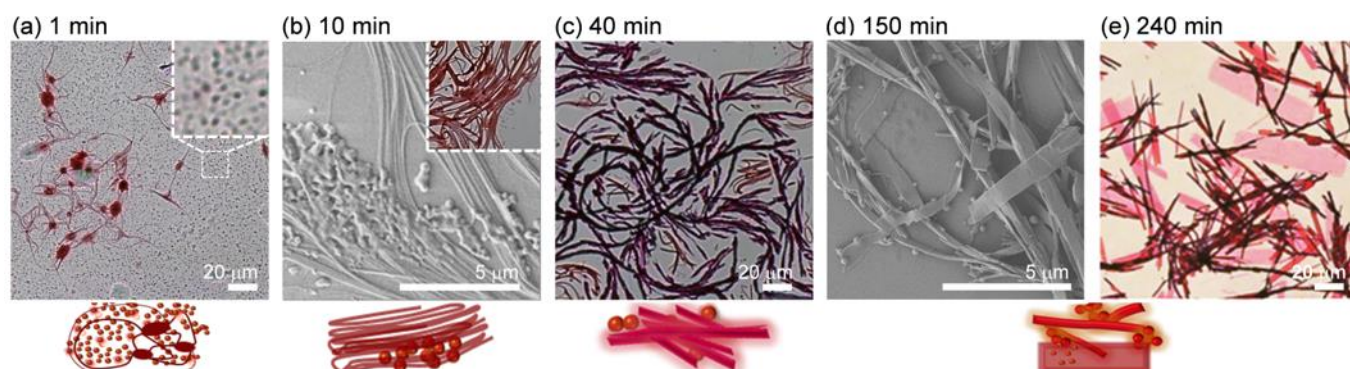


Figure 7. OM (a, inset image in b,c,e) and SEM (b,d) images showing the morphological growth processes of 3Bu THF-H₂O (1/1, *v/v*) mixtures according to storage time at 10–15 °C.

2.5. FT-IR and XRD Measurements

Fourier-transform infrared (FT-IR) and X-ray diffraction (XRD) experiments were performed to obtain useful information on (i) the molecular structures and (ii) the degree of molecular arrangement responsible for the respective spherical and 1D assemblies. Importantly, a weak band maximized at around 1730 cm⁻¹ and a quite broad band at 3100–3500 cm⁻¹ emerged in the IR spectrum of intertwined fiber samples produced from toluene-MeOH mixtures (Figure 8a), and they could be attributed to carbonyl stretching and hydrogen bonding, respectively [79–81]. Rather than a typical ketone, the carbonyl is considered to experience ring strain or to be close to an electron-withdrawing substituent [79,80]. For confirmation, we reproduced such 1D structures in the same manner and dried them in a vacuum for 6 days to sufficiently remove residual solvents. The obtained sample also exhibited the same absorption band. These results indicate that a considerable amount of the hydrazone form present in a toluene solution was retained even after fiber formation.

By contrast, the IR spectrum of the spherical aggregates displayed an aromatic C-H stretching vibration at around 3011 cm⁻¹ and aromatic C=C stretching bands at 1601 and 1484 cm⁻¹, but did not show any absorption bands corresponding to the carbonyl stretching mode. It is thus reasonable to interpret that a significant amount of 3Bu, which existed in the twisted azo form rather than in the hydrazone form, tended to assemble quickly into less ordered spherical structures.

In contrast to spheres showing soft and weak signals, sharp and higher-intensity peaks were recorded in the XRD pattern for the crystalline fibrous structures (Figure 8b), as predicted earlier. The sharp and strongest signal appeared near $2\theta = 4.26^\circ$ ($d = 2.08$ nm), which is slightly shorter than the full molecular length (2.15 nm) predicted by the theoretical calculation. On the other hand, the sphere sample showed almost the same XRD pattern as in the previous report [60], and had a strong peak at $2\theta = 4.12^\circ$ ($d = 2.14$ nm) corresponding to the molecular length. Fairly weak peaks appeared at $2\theta = 19.58^\circ$ ($d = 0.45$ nm) and 23.33° ($d = 0.38$ nm), reflecting that intermolecular distances were longer than those of typical π - π stacking interactions between planar aromatic units [82–85]. In addition, such broad peaks were rarely observed in the XRD pattern of crystalline fiber samples. This can be interpreted as follows. The triangular 3Bu molecule with three bulky *ortho*-alkylated biphenyl wings is highly sterically crowded [63–66,86–89], and intramolecular rotation around a single or double bond is greatly restricted. As a result, considerable occupied space per molecule is secured, and intermolecular interactions are weakened. For this reason, although dense packing is difficult, it appears that conditions for the molecules to grow into spherical and one-dimensional structures in the mixed solutions were provided.

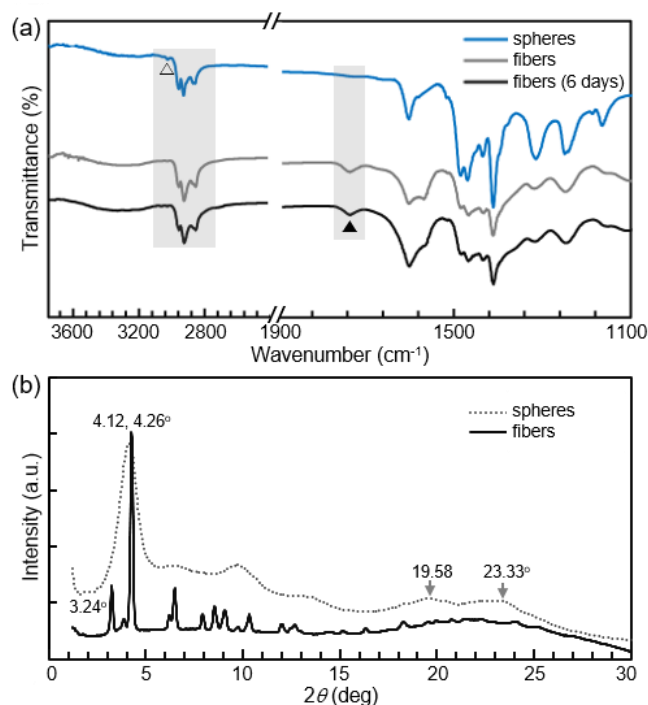


Figure 8. (a) FT-IR and (b) XRD patterns of spherical and 1D fibrous structures in (a), “6 days” denotes a sample dried in a vacuum for 6 days.

2.6. Fluorescence Switching Accompanied by Morphological Transition

To realize reversible fluorescence switching of less ordered spheres with AIEE characteristics, between on and off states, we devised an experimental method to utilize the result that the visible light-induced sphere-to-liquid phase transition is accompanied by fluorescence on-to-off switching (the fluorescence quantum yield (Φ_f) decreased from 2.4% to \sim 0.4%). We assumed that, if a light-irradiated sample is exposed to solvent vapor, the movement of 3Bu molecules becomes more random due to intermolecular interactions between chromophore and solvent molecules. However, if the molecular arrangements in the spherical aggregates could be maintained to some extent, because the spatial arrangements of the 3Bu molecules could be amplified during the drying process after exposure to solvent vapor, the original shape could be restored to some extent. To test this assumption, we exposed a green-light-irradiated sphere sample to THF vapor (with a low boiling temperature) in a sealed bottle (Figure 9). When the sample was removed from the bottle after 3 hours and slowly dried at ambient temperature, the original round shape was restored. At the same time, the fluorescence intensity also improved ($\Phi_f = \sim$ 1.9%). However, if the sample was exposed to solvent vapor for too long (Figure S5) and the spatial arrangements disappeared completely, it was almost impossible to achieve sufficient morphological recovery.

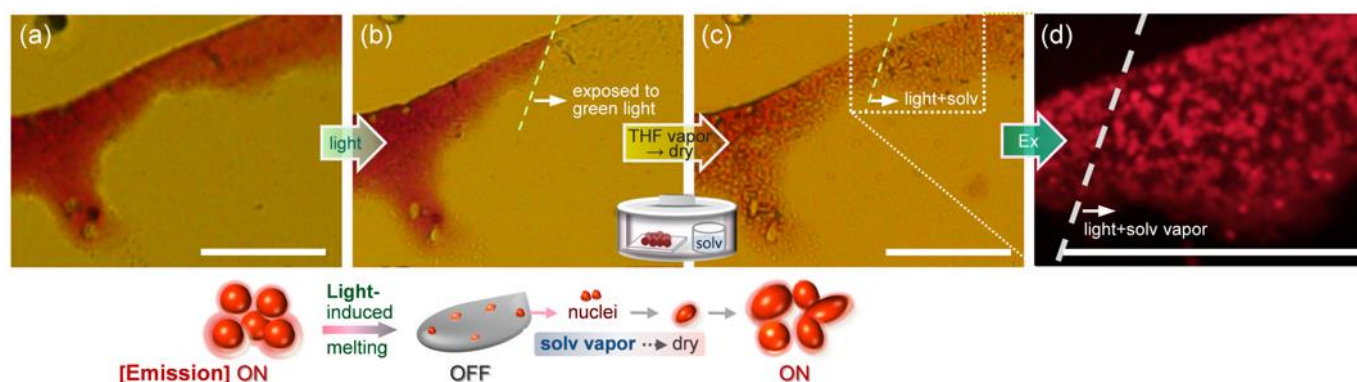


Figure 9. Reversible fluorescence switching: When spherical aggregates on a quartz substrate were exposed to (a,b) visible (green) light, a significant color change (due to light-induced melting) occurred with a reduction in the fluorescence intensity. (c) OM and corresponding (d) magnified FOM images taken after exposure of the sphere sample to THF vapor for 3 hours. Their morphological recovery caused the sample to fluoresce again. Scale bar: 50 μm .

3. Conclusions

We investigated the relationship between (i) the conformational and tautomeric structure in which a triangular chromophore preferentially is adopted depending on the solvent polarity and the concentration, (ii) the resulting spectroscopic features, and (iii) self-assembled nano-, micro-, and macrostructures formed in various mixed solutions. The combination of our experimental results and theoretical calculations revealed that, in a very dilute DMF solution, the triangular molecule present in a highly twisted azo form tended to assemble into less ordered spherical nanoparticles or microspheres. In contrast, in non-polar toluene solutions, the polar central ring part adopted a more planar form, thereby promoting conversion to the hydrazone form. The resulting tautomer grew slowly into crystalline micro- and millimeter-sized 1D structures. Interestingly, upon storing the THF-H₂O mixtures at a low temperature, birefringent 2D sheets were created through the lateral stacking of elongated fibers. Furthermore, the shape and fluorescence intensity of sphere samples could change in response to stimuli such as light and solvent vapor. These findings may be useful for developing new fluorescent materials for chemical detection as well as for rewritable data storage.

4. Materials and Methods

4.1. Materials

Spectroscopic grade organic solvents (N,N-dimethylformamide (DMF), tetrahydrofuran (THF), toluene, methanol (MeOH), chloroform) were purchased from Kanto Chemical Co., INC, Japan. Ultrapure water (which was purified to reach a minimum resistivity of 18.0 M Ω ·cm (25 °C) using a μ Pure HIQ water purification system, Romax, South Korea) was utilized in all experiments.

4.2. Characterization

After a 30 s nitrogen purge, a screw-cap quartz cuvette containing 3Bu solution was sealed with Parafilm[®]. UV-vis absorption and fluorescence spectra were obtained using a Shimadzu UV-2600 UV-vis spectrophotometer (Shimadzu Corporation, Kyoto, Japan) and a Horiba FluoroMax-4 spectrofluorometer (Horiba Ltd., Japan), respectively. Optical microscopy (OM) and fluorescence optical microscopy (FOM, $\lambda_{\text{ex}} = 520\text{--}550\text{ nm}$) experiments were performed using an Olympus BX53 microscope after placing two to three drops of 3Bu mixed suspension onto a clean glass or quartz substrate. Polarized optical microscopy (POM) images were obtained using an Olympus BX53-P polarizing microscope (Olympus Corporation, Tokyo, Japan). Atomic force microscopy (AFM) measurements were performed using XE-100 (PSIA, Corp., Korea) equipped with a 50 μm

scanner. FE-SEM (field-emission scanning electron microscopy: HITACHI SU8020 (Hitachi High-Technologies Corporation, Tokyo, Japan) and TESKAN-MIRA3-LM (TESCAN ORSAY HOLDING, a.s., Czech Republic) samples were coated with an approximately 5–10 nm thick platinum layer using a Cressington 108 auto sputter coater (Ted Pella, Inc., CA, USA). The thermal stability of 3Bu was determined by a thermogravimetric analysis (TGA) method using a Pyris 1TGA Thermogravimetric Analyzer (PerkinElmer, Inc., Waltham, MA, USA). All measurements were performed under a nitrogen atmosphere in a temperature range of 22 to 490 °C. All experiments were performed twice at a heating rate of 5 °C/min. Fourier transform infrared (FT-IR) spectra were recorded on a PerkinElmer (spectrum 100) spectrometer. X-ray diffraction (XRD) data were collected with Cu K α radiation on Rigaku R-AXIS-IV and R-AXIS-VII X-ray imaging plate detectors to determine the structure of the 3Bu molecule.

Supplementary Materials: The following supporting information can be downloaded at: <https://www.mdpi.com/article/10.3390/ijms23020965/s1>.

Author Contributions: M.H. (Mina Han) conceived the experiments. I.A. and M.H. (Mina Han) performed the spectroscopic, OM, FOM, SEM, FT-IR and XRD measurements. J.O. and J.J. carried out and interpreted the density functional theory (DFT) calculations. Y.J.S. and J.N. performed AFM measurements. M.H. (Mitsuo Hara) and T.S. performed XRD observations. M.H. (Mina Han) and J.J. prepared the manuscript. All authors have read and agreed to the published version of the manuscript.

Funding: This work was supported by grants from the National Research Foundation (NRF) of Korea (2018R1A2B6009315) and the framework of bilateral international cooperation program managed by the NRF-Japan Society for the Promotion of Science (2018K2A9A2A08000191).

Institutional Review Board Statement: Not applicable.

Informed Consent Statement: Not applicable.

Data Availability Statement: The data are included within the manuscript and Supplementary Materials.

Acknowledgments: We are grateful to Yeong-Jun Lee (KNU) for his assistance with FE-SEM measurements.

Conflicts of Interest: The authors declare no conflict of interest.

References

1. Palmer, L.; Stupp, S.I. Molecular Self-Assembly into One-Dimensional Nanostructures. *Acc. Chem. Res.* **2008**, *41*, 1674–1684. [[CrossRef](#)]
2. Sagara, Y.; Kato, T. Mechanically induced luminescence changes in molecular assemblies. *Nat. Chem.* **2009**, *1*, 605–610. [[CrossRef](#)]
3. Zhao, Y.S.; Fu, H.; Peng, A.; Ma, Y.; Liao, Q.; Yao, J. Construction and Optoelectronic Properties of Organic One-Dimensional Nanostructures. *Acc. Chem. Res.* **2010**, *43*, 409–418. [[CrossRef](#)]
4. de Rooy, S.L.; El-Zahab, B.; Li, M.; Das, S.; Broering, E.; Chandler, L.; Warner, I.M. Fluorescent one-dimensional nanostructures from a group of uniform materials based on organic salts. *Chem. Commun.* **2011**, *47*, 8916–8918. [[CrossRef](#)]
5. Cantekin, S.; Greef, T.F.A.; Palmans, A.R.A. Benzene-1,3,5-Tricarboxamide: A Versatile Ordering Moiety for Supramolecular Chemistry. *Chem. Soc. Rev.* **2012**, *41*, 6125–6137. [[CrossRef](#)]
6. Kim, Y.; Li, W.; Shin, S.; Lee, M. Development of Toroidal Nanostructures by Self-Assembly: Rational Designs and Applications. *Acc. Chem. Res.* **2013**, *46*, 2888–2897. [[CrossRef](#)]
7. Wei, R.; Song, P.; Tong, A. Reversible Thermochromism of Aggregation-Induced Emission-Active Benzophenone Azine Based on Polymorph-Dependent Excited-State Intramolecular Proton Transfer Fluorescence. *J. Phys. Chem. C* **2013**, *117*, 3467–3474. [[CrossRef](#)]
8. Kim, H.-J.; Whang, D.R.; Gierschner, J.; Lee, C.H.; Park, S.Y. High-Contrast Red-Green-Blue Tricolor Fluorescence Switching in Bicomponent Molecular Film. *Angew. Chem. Int. Ed.* **2015**, *54*, 4330–4333. [[CrossRef](#)]
9. Ito, S.; Yamada, T.; Taguchi, T.; Yamaguchi, Y.; Asami, M. N-Boc-Indolylbenzothiadiazole Derivatives: Efficient Full-Color Solid-State Fluorescence and Self-Recovering Mechanochromic Luminescence. *Chem. Asian J.* **2016**, *11*, 1963–1970. [[CrossRef](#)] [[PubMed](#)]
10. Yang, W.; Liu, C.; Lu, S.; Du, J.; Gao, Q.; Zhang, R.; Liu, Y.; Yang, C. Smart On-Off Switching Luminescence Materials with Reversible Piezochromism and Basichromism. *ChemistrySelect* **2017**, *2*, 9215–9221. [[CrossRef](#)]

11. Rosbottom, I.; Ma, C.Y.; Turner, T.D.; O'Connell, R.A.; Loughrey, J.; Sadiq, G.; Davey, R.J.; Roberts, K.J. Influence of Solvent Composition on the Crystal Morphology and Structure of p Aminobenzoic Acid Crystallized from Mixed Ethanol and Nitromethane Solutions. *Cryst. Growth Des.* **2017**, *17*, 4151–4161. [[CrossRef](#)]
12. Han, M.; Abe, I.; Matsuura, K.; Takeoka, Y.; Seki, T. Morphologically Diverse Micro- and Macrostructures Created via Solvent Evaporation-Induced Assembly of Fluorescent Spherical Particles in the Presence of Polyethylene Glycol Derivatives. *Molecules* **2021**, *26*, 4294. [[CrossRef](#)] [[PubMed](#)]
13. Nador, F.; Wnuk, K.; Roscini, C.; Solorzano, R.; Farauo, J.; Ruiz-Molina, D.; Novio, F. Solvent-Tuned Supramolecular Assembly of Fluorescent Catechol/Pyrene Amphiphilic Molecules. *Chem. Eur. J.* **2018**, *24*, 14724–14732. [[CrossRef](#)]
14. Zheng, D.; Gu, Y.; Li, X.; Zhang, L.; Zhao, W.; Ma, J. Hydrogen Bonding Promoted Tautomerism between Azo and Hydrazone Forms in Calcon with Multistimuli Responsiveness and Biocompatibility. *J. Chem. Inf. Model.* **2019**, *59*, 2110–2122. [[CrossRef](#)]
15. Peng, H.; Liu, B.; Liu, J.; Wei, P.; Zhang, H.; Han, T.; Qi, J.; Lam, J.W.Y.; Zhang, W.; Tang, B.Z. "Seeing" and Controlling Photoisomerization by (Z) / (E) Isomers with Aggregation-Induced Emission Characteristics. *ACS Nano* **2019**, *13*, 12120–12126. [[CrossRef](#)]
16. Castillo-Vallés, M.; Martínez-Bueno, A.; Giménez, R.; Sierra, T.; Ros, M.B. Beyond liquid crystals: New research trends for mesogenic molecules in liquids. *J. Mater. Chem. C* **2019**, *7*, 14454–14470. [[CrossRef](#)]
17. Shen, B.; Kim, Y.; Lee, M. Supramolecular Chiral 2D Materials and Emerging Functions. *Adv. Mater.* **2020**, *32*, e1905669. [[CrossRef](#)]
18. Zhou, S.; Guo, S.; Liu, W.; Yang, Q.; Sun, H.; Ding, R.; Qian, Z.; Feng, H. Rational design of reversibly photochromic molecules with aggregation-induced emission by introducing photoactive thienyl and benzothienyl groups. *J. Mater. Chem. C* **2020**, *8*, 13197–13204. [[CrossRef](#)]
19. Yang, M.; Park, I.S.; Miyashita, Y.; Tanaka, K.; Yasuda, T. Mechanochromic Delayed Fluorescence Switching in Propeller-Shaped Carbazole–Isophthalonitrile Luminogens with Stimuli-Responsive Intramolecular Charge-Transfer Excited States. *Angew. Chem. Int. Ed.* **2020**, *59*, 13955–13961. [[CrossRef](#)]
20. Kumar, R.; Aggarwal, H.; Srivastava, A. Of Twists and Curves: Electronics, Photophysics, and Upcoming Applications of Non-Planar Conjugated Organic Molecules. *Chem. Eur. J.* **2020**, *26*, 10653–10675. [[CrossRef](#)]
21. Barman, D.; Gogoi, R.; Narang, K.; Iyer, P.K. Recent Developments on Multi-Functional Metal-Free Mechanochromic Luminescence and Thermally Activated Delayed Fluorescence Organic Materials. *Front. Chem.* **2020**, *8*, 483. [[CrossRef](#)] [[PubMed](#)]
22. Yamashita, M.; Nagai, S.; Ito, S.; Tachikawa, T. In Situ Exploration of Stimulus-Induced Emission Changes in Mechanochromic Dyes. *J. Phys. Chem. Lett.* **2021**, *12*, 7826–7831. [[CrossRef](#)] [[PubMed](#)]
23. Chiriac, F.; Iliş, M.; Madalan, A.; Manaila-Maximean, D.; Secu, M.; Cîrcu, V. Thermal and Emission Properties of a Series of Lanthanides Complexes with N-Biphenyl-Alkylated-4-Pyridone Ligands: Crystal Structure of a Terbium Complex with N-Benzyl-4-Pyridone. *Molecules* **2021**, *26*, 2017. [[CrossRef](#)] [[PubMed](#)]
24. Chiriac, L.F.; Ganea, P.C.; Manaila-Maximean, D.; Pasuk, I.; Cîrcu, V. Synthesis and thermal, emission and dielectric properties of liquid crystalline Eu(III), Sm(III) and Tb(III) complexes based on mesogenic 4-pyridone ligands functionalized with cyano-biphenyl groups. *J. Mol. Liq.* **2019**, *290*, 111184. [[CrossRef](#)]
25. Ilinca, T.A.; Manaila-Maximean, D.; Ganea, P.C.; Pasuk, I.; Cîrcu, V. Polarized emission and dielectric studies of novel lanthanidomesogens based on 4-pyridone ligands. In Proceedings of the Advanced Topics in Optoelectronics, Microelectronics and Nanotechnologies X, Constanta, Romania, 20–23 August 2020; Volume 11718, p. 117182U.
26. Reichardt, C. Solvatochromic Dyes as Solvent Polarity Indicators. *Chem. Rev.* **1994**, *94*, 2319–2358. [[CrossRef](#)]
27. Nigam, S.; Rutan, S. Principles and Applications of Solvatochromism. *Appl. Spectrosc.* **2001**, *55*, 362A–370A. [[CrossRef](#)]
28. Jin, Q.; Zhang, L.; Liu, M. Solvent-Polarity-Tuned Morphology and Inversion of Supramolecular Chirality in a Self-Assembled Pyridylpyrazole-Linked Glutamide Derivative: Nanofibers, Nanotwists, Nanotubes, and Microtubes. *Chem. A Eur. J.* **2013**, *19*, 9234–9241. [[CrossRef](#)]
29. Niu, C.; You, Y.; Zhao, L.; He, D.; Na, N.; Ouyang, J. Solvatochromism, Reversible Chromism and Self-Assembly Effects of Heteroatom-Assisted Aggregation-Induced Enhanced Emission (AIEE) Compounds. *Chem. Eur. J.* **2015**, *21*, 13983–13990. [[CrossRef](#)]
30. Zhao, J.; Sun, J.; Simalou, O.; Wang, H.; Peng, J.; Zhai, L.; Xue, P.; Lu, R. Multi-stimuli-responsive fluorescent aminostyrylquinoxalines: Synthesis, solvatochromism, mechanofluorochromism and acidochromism. *Dyes Pigm.* **2018**, *151*, 296–302. [[CrossRef](#)]
31. Balam-Villarreal, J.A.; López-Mayorga, B.J.; Gallardo-Rosas, D.; Toscano, R.A.; Carreón-Castro, M.P.; Basiuk, V.A.; Cor-tés-Guzmán, F.; López-Cortés, J.G.; Ortega-Alfaro, M.C. π -Extended push-pull azo-pyrrole photoswitches: Synthesis, solvatochromism and optical band gaps. *Org. Biomol. Chem.* **2020**, *18*, 1657–1670. [[CrossRef](#)]
32. Murata, K.; Aoki, M.; Suzuki, T.; Harada, T.; Kawabata, H.; Komori, T.; Ohseto, F.; Ueda, K.; Shinkai, S. Thermal and Light Control of the Sol-Gel Phase Transition in Cholesterol-Based Organic Gels. Novel Helical Aggregation Modes as Detected by Circular Dichroism and Electron Microscopic Observation. *J. Am. Chem. Soc.* **1994**, *116*, 6664–6676. [[CrossRef](#)]
33. Abendroth, J.M.; Bushuyev, O.S.; Weiss, P.S.; Barrett, C.J. Controlling Motion at the Nanoscale: Rise of the Molecular Machines. *ACS Nano* **2015**, *9*, 7746–7768. [[CrossRef](#)] [[PubMed](#)]
34. Pires, A.C.; Soares, N.D.F.F.; Da Silva, L.H.M.; Da Silva, M.C.H.; Mageste, A.B.; Soares, R.F.; Teixeira, A.V.N.C.; Andrade, N.J. Thermodynamic Study of Colorimetric Transitions in Polydiacetylene Vesicles Induced by the Solvent Effect. *J. Phys. Chem. B* **2010**, *114*, 13365–13371. [[CrossRef](#)]

35. Kaszyńska, J.; Łapiński, A.; Bielejewski, M.; Luboradzki, R.; Tritt-Goc, J. On the relation between the solvent parameters and the physical properties of methyl-4,6-O-benzylidene- α -d-glucopyranoside organogels. *Tetrahedron* **2012**, *68*, 3803–3810. [[CrossRef](#)]
36. Zhu, N.; Yan, Q.; Luo, Z.; Zhai, Y.; Zhao, D. Helical Folding of Conjugated Oligo(phenyleneethynylene): Chain-Length Dependence, Solvent Effects, and Intermolecular Assembly. *Chem. Asian J.* **2012**, *7*, 2386–2393. [[CrossRef](#)] [[PubMed](#)]
37. Würthner, F. Solvent Effects in Supramolecular Chemistry: Linear Free Energy Relationships for Common Intermolecular Interactions. *J. Org. Chem.* **2021**. [[CrossRef](#)]
38. Rau, H. *Photochromism, Molecules and Systems*; Dürr, H., Buuas-Laurent, H., Eds.; Elsevier: Amsterdam, The Netherlands, 1990.
39. Sekkat, Z.; Knoll, W. *Photoreactive Organic thin Films in the Light of Bound Electromagnetic Waves*; John and Wiley and Sons: Hoboken, NJ, USA, 1997; pp. 117–195.
40. Rau, H. Spectroscopic properties of organic azo compounds, *Angew. Chem. Int. Ed. Engl.* **1973**, *12*, 224. [[CrossRef](#)]
41. Morgante, C.G.; Struve, W.S. S₂→S₀ fluorescence in trans-azobenzene. *Chem. Phys. Lett.* **1979**, *68*, 267–271. [[CrossRef](#)]
42. Azuma, J.; Tamai, N.; Shishido, A.; Ikeda, T. Femtosecond dynamics and stimulated emission from the S₂ state of a liquid crystalline trans-azobenzene. *Chem. Phys. Lett.* **1998**, *288*, 77–82. [[CrossRef](#)]
43. Satzger, H.; Spörlein, S.; Root, C.; Wachtveitl, J.; Zinth, W.; Gilch, P. Fluorescence spectra of trans- and cis-azobenzene—emission from the Franck–Condon state. *Chem. Phys. Lett.* **2003**, *372*, 216–223. [[CrossRef](#)]
44. Yoshino, J.; Kano, N.; Kawashima, T. Synthesis of the most intensely fluorescent azobenzene by utilizing the B–N interaction. *Chem. Commun.* **2007**, 559–561. [[CrossRef](#)] [[PubMed](#)]
45. Yoshino, J.; Furuta, A.; Kambe, T.; Itoi, H.; Kano, N.; Kawashima, T.; Ito, Y.; Asashima, M. Intensely Fluorescent Azobenzenes: Synthesis, Crystal Structures, Effects of Substituents, and Application to Fluorescent Vital Stain. *Chem. Eur. J.* **2010**, *16*, 4951. [[CrossRef](#)]
46. Yoshino, J.; Kano, N.; Kawashima, T. Fluorescent azobenzenes and aromatic aldimines featuring an N–B interaction. *Dalton Trans.* **2013**, *42*, 15826. [[CrossRef](#)]
47. Luo, J.; Xie, Z.; Lam, J.W.Y.; Cheng, L.; Chen, H.; Qiu, C.; Kwok, H.S.; Zhan, X.; Liu, Y.; Zhu, D.; et al. Aggregation-Induced Emission of 1-Methyl-1,2,3,4,5-Pentaphenylsilole. *Chem. Commun.* **2001**, *18*, 174–1741. [[CrossRef](#)]
48. An, B.-K.; Kwon, S.-K.; Jung, S.-D.; Park, S.Y. Enhanced Emission and Its Switching in Fluorescent Organic Nanoparticles. *J. Am. Chem. Soc.* **2002**, *124*, 14410–14415. [[CrossRef](#)] [[PubMed](#)]
49. An, B.-K.; Gierschner, J.; Park, S.Y. π -Conjugated Cyanostilbene Derivatives: A Unique Self-Assembly Motif for Molecular Nanostructures with Enhanced Emission and Transport. *Acc. Chem. Res.* **2012**, *45*, 544–554. [[CrossRef](#)]
50. Gopikrishna, P.; Meher, N.; Iyer, P.K. Functional 1,8-Naphthalimide AIE/AIEEgens: Recent Advances and Prospects. *ACS Appl. Mater. Interfaces* **2018**, *10*, 12081–12111. [[CrossRef](#)] [[PubMed](#)]
51. Li, J.; Wang, J.; Li, H.; Song, N.; Wang, D.; Tang, B.Z. Supramolecular materials based on AIE luminogens (AIEgens): Construction and applications. *Chem. Soc. Rev.* **2020**, *49*, 1144–1172. [[CrossRef](#)]
52. Li, Z.; Ji, X.; Xie, H.; Tang, B.Z. Aggregation-Induced Emission-Active Gels: Fabrications, Functions, and Applications. *Adv. Mater.* **2021**, *33*, 2100021. [[CrossRef](#)] [[PubMed](#)]
53. Yoon, Y.; Jo, S.; Park, S.J.; Kim, H.M.; Kim, D.; Lee, T.S. Unusual fluorescence of o-phenylazonaphthol derivatives with aggregation-induced emission and their use in two-photon cell imaging. *Chem. Commun.* **2019**, *55*, 6747–6750. [[CrossRef](#)]
54. Yamauchi, M.; Yokoyama, K.; Aratani, N.; Yamada, H.; Masuo, S. Crystallization-Induced Emission of Azobenzene Derivatives. *Angew. Chem. Int. Ed.* **2019**, *58*, 14173–14178. [[CrossRef](#)]
55. Diana, R.; Caruso, U.; Piotta, S.; Concilio, S.; Shikler, R.; Panunzi, B. Spectroscopic Behaviour of Two Novel Azobenzene Fluorescent Dyes and Their Polymeric Blends. *Molecules* **2020**, *25*, 1368. [[CrossRef](#)]
56. Lee, H.Y.; Song, X.; Park, H.; Baik, M.-H.; Lee, D. Torsionally Responsive C₃-Symmetric Azo Dyes: Azo–Hydrazone Tautomerism, Conformational Switching, and Application for Chemical Sensing. *J. Am. Chem. Soc.* **2010**, *132*, 12133–12144. [[CrossRef](#)] [[PubMed](#)]
57. Lim, S.-J.; An, B.-K.; Jung, S.D.; Chung, M.-A.; Park, S.Y. Photoswitchable Organic Nanoparticles and a Polymer Film Employing Multifunctional Molecules with Enhanced Fluorescence Emission and Bistable Photochromism. *Angew. Chem. Int. Ed.* **2004**, *43*, 6346–6350. [[CrossRef](#)] [[PubMed](#)]
58. Herbert, K.; Schrettl, S.; Rowan, S.J.; Weder, C. 50th Anniversary Perspective: Solid-State Multistimuli, Multiresponsive Polymeric Materials. *Macromolecules* **2017**, *50*, 8845–8870. [[CrossRef](#)]
59. Han, T.; Yao, Z.; Qiu, Z.; Zhao, Z.; Wu, K.; Wang, J.; Poon, A.W.; Lam, J.W.Y.; Tang, B.Z. Photoresponsive spiro-polymers generated in situ by C–H-activated polyspiroannulation. *Nat. Commun.* **2019**, *10*, 1–11. [[CrossRef](#)] [[PubMed](#)]
60. Abe, I.; Hara, M.; Seki, T.; Cho, S.J.; Shimizu, M.; Matsuura, K.; Cheong, H.-K.; Kim, J.Y.; Oh, J.; Jung, J.; et al. A trigonal molecular assembly system with the dual light-driven functions of phase transition and fluorescence switching. *J. Mater. Chem. C* **2019**, *7*, 2276–2282. [[CrossRef](#)]
61. Luo, W.; Wang, G. Photo-Responsive Fluorescent Materials with Aggregation-Induced Emission Characteristics. *Adv. Opt. Mater.* **2020**, *8*, 2001362. [[CrossRef](#)]
62. Xue, L.; Pan, Y.; Zhang, S.; Chen, Y.; Yu, H.; Yang, Y.; Mo, L.; Sun, Z.; Li, L.; Yang, H. Fluorescent Azobenzene-Containing Compounds: From Structure to Mechanism. *Crystals* **2021**, *11*, 840. [[CrossRef](#)]
63. Forber, C.L.; Kelusky, E.C.; Bunce, N.J.; Zerner, M.C. Electronic spectra of cis- and trans-azobenzenes: Consequences of ortho substitution. *J. Am. Chem. Soc.* **1985**, *107*, 5884–5890. [[CrossRef](#)]

64. Beharry, A.A.; Sadovski, O.; Woolley, G.A. Azobenzene Photoswitching without Ultraviolet Light. *J. Am. Chem. Soc.* **2011**, *133*, 19684–19687. [CrossRef]
65. Han, M.; Cho, S.J.; Norikane, Y.; Shimizu, M.; Kimura, A.; Tamagawa, T.; Seki, T. Multistimuli-responsive azobenzene nan-ofibers with aggregation-induced emission enhancement characteristics. *Chem. Commun.* **2014**, *50*, 15815–15818. [CrossRef]
66. Dong, M.; Babalhavaeji, A.; Samanta, S.; Beharry, A.A.; Woolley, G.A. Red-Shifting Azobenzene Photoswitches for in Vivo Use. *Acc. Chem. Res.* **2015**, *48*, 2662–2670. [CrossRef]
67. Gabor, G.; Frei, Y.; Gegiou, D.; Kaganowitch, M.; Fischer, E. Tautomerism and Geometric Isomerism in Arylazo-Phenols and Naphthols. Part III. Orthohydroxy Derivatives and their Reversible Photochemical Reactions. *Isr. J. Chem.* **1967**, *5*, 193–211. [CrossRef]
68. Douhal, A.; Sanz, M.; Tormo, L. Femtochemistry of orange II in solution and in chemical and biological nanocavities. *Proc. Natl. Acad. Sci. USA* **2005**, *102*, 18807–18812. [CrossRef]
69. Cui, G.; Guan, P.-J.; Fang, W.-H. Photoinduced Proton Transfer and Isomerization in a Hydrogen-Bonded Aromatic Azo Compound: A CASPT2//CASSCF Study. *J. Phys. Chem. A* **2014**, *118*, 4732–4739. [CrossRef]
70. Ghasemian, M.; Kakanejadifard, A.; Azarbani, F.; Zabardasti, A.; Kakanejadifard, S. Spectroscopy and solvatochromism studies along with antioxidant and antibacterial activities investigation of azo-azomethine compounds 2-(2-hydroxyphenylimino)methyl-4-phenyldiazenylphenol. *Spectrochim. Acta Part A Mol. Biomol. Spectrosc.* **2014**, *124*, 153–158. [CrossRef] [PubMed]
71. Rauf, M.A.; Hisaindee, S.; Saleh, N. Spectroscopic studies of keto-enol tautomeric equilibrium of azo dyes. *RSC Adv.* **2015**, *5*, 18097–18110. [CrossRef]
72. Adamo, C.; Barone, V. Toward reliable density functional methods without adjustable parameters: The PBE0 model. *J. Chem. Phys.* **1999**, *110*, 6158–6170. [CrossRef]
73. Frisch, M.J.; Trucks, G.W.; Schlegel, H.B.; Scuseria, G.E.; Robb, M.A.; Cheeseman, J.R.; Scalmani, G.; Barone, V.; Mennucci, B.; Petersson, G.A.; et al. *Gaussian 09, Revision E.01*; Gaussian, Inc.: Wallingford, CT, USA, 2009.
74. Marenich, A.V.; Cramer, C.J.; Truhlar, D.G. Pacific Northwest National Laboratory (PNNL), Richland, WA (US), Environmental Molecular Sciences Laboratory (EMSL) Universal Solvation Model Based on Solute Electron Density and on a Continuum Model of the Solvent Defined by the Bulk Dielectric Constant and Atomic Surface Tensions. *J. Phys. Chem. B* **2009**, *113*, 6378.
75. Polarized Light Microscopy. Available online: <https://www.microscopyu.com/techniques/polarized-light/polarized-light-microscopy> (accessed on 10 December 2021).
76. Fukuhara, K.; Nagano, S.; Hara, M.; Seki, T. Free-surface molecular command systems for photoalignment of liquid crystalline materials. *Nat. Commun.* **2014**, *5*, 3320. [CrossRef]
77. Han, M.; Hirade, T. Anisotropic two-dimensional sheets assembled from rod-shaped metal complexes. *Chem. Commun.* **2012**, *48*, 100–102. [CrossRef]
78. Bäcklund, F.G.; Elfving, A.; Musumeci, C.; Ajjan, F.; Babenko, V.; Dzwolak, W.; Solin, N.; Inganäs, O. Conducting microhelices from self-assembly of protein fibrils. *Soft Matter* **2017**, *13*, 4412–4417. [CrossRef] [PubMed]
79. Pavia, D.L.; Lampan, G.M.; Kriz, G.S. *Introduction to Spectroscopy*; W.B. Saunders Company: Philadelphia, PA, USA, 1979.
80. Guenzler, H.; Gremlich, H.; Bluemich, M. *IR Spectroscopy: An Introduction*; Wiley-VCH: Weinheim, Germany, 2002.
81. Han, M.; Ichimura, K. In-Plane and Tilt Reorientation of *p*-Methoxyazobenzene Side Chains Tethered to Liquid Crystalline Polymethacrylates by Irradiation with 365 nm Light. *Macromolecules* **2001**, *34*, 90–98. [CrossRef]
82. Iijima, S.; Ichibashi, T. Single-shell carbon nanotubes of 1-nm diameter. *Nature* **1993**, *363*, 603. [CrossRef]
83. Davis, R.; Rath, N.P.; Das, S. Thermally reversible fluorescent polymorphs of alkoxy-cyano-substituted diphenylbutadienes: Role of crystal packing in solid state fluorescence. *Chem. Commun.* **2004**, 74–75. [CrossRef] [PubMed]
84. Hill, J.P.; Jin, W.; Kosaka, A.; Fukushima, T.; Ichihara, H.; Shimomura, T.; Ito, K.; Hashizume, T.; Ishii, N.; Aida, T. Self-Assembled Hexa- peri -hexabenzocoronene Graphitic Nanotube. *Science* **2004**, *304*, 1481–1483. [CrossRef]
85. Mena-Osteritz, E. Superstructures of Self-Organizing Thiophenes. *Adv. Mater.* **2002**, *14*, 609–616. [CrossRef]
86. Bunce, N.J.; Ferguson, G.; Forber, C.L.; Stachnyk, G.J. Sterically Hindered Azobenzenes: Isolation of Cis Isomers and Kinetics of Thermal Cis → Trans Isomerization. *J. Org. Chem.* **1987**, *52*, 394–398. [CrossRef]
87. Han, M.R.; Hashizume, D.; Hara, M. 1-[(E)-3-sec-Butyl-4-(4'-ethoxy-3,5-diethylbiphenyl-4-yl diazenyl)phenoxy]hexadecane. *Acta Crystallogr. Sect. E Struct. Rep. Online* **2006**, *62*, o3001–o3003. [CrossRef]
88. Hirade, T.; Okui, Y.; Han, M. A design strategy for stable light-sensitive palladium complexes. *J. Mater. Chem. C* **2013**, *1*, 2672–2679. [CrossRef]
89. Lameijer, L.N.; Budzak, S.; Simeth, N.A.; Hansen, M.J.; Feringa, B.L.; Jacquemin, D.; Szymanski, W. General Principles for the Design of Visible-Light-Responsive Photoswitches: Tetra-ortho-Chloro-Azobenzenes. *Angew. Chem. Int. Ed.* **2020**, *59*, 21663–21670. [CrossRef] [PubMed]